ARTICLE

OBC
www.rsc.org/obc

NMR conformational analysis of biosynthetic precursor-type lipid A: monomolecular state and supramolecular assembly†

Masato Oikawa, Tetsuya Shintaku, Naohiro Fukuda, Harald Sekljic, Yoshiyuki Fukase, Hiroaki Yoshizaki, Koichi Fukase* and Shoichi Kusumoto

Department of Chemistry, Graduate School of Science, Osaka University, 1-1 Machikaneyama, Toyonaka, Osaka, 560-0043, Japan. E-mail: koichi@chem.sci.osaka-u.ac.jp

Received 12th July 2004, Accepted 30th September 2004
First published as an Advance Article on the web 8th November 2004

The detailed conformational analysis of a single molecule of the tetraacyl biosynthetic precursor-type lipid A and its characteristic supramolecular assembly in aqueous SDS-micelles are described. Regular molecular arrangements were observed by detailed analysis of the NMR spectra of synthetically pure specimens, including regiospecifically ^{13}C-labeled ones. NMR analysis of a biologically inactive precursor-type analogue with four shorter acyl chains demonstrated its conformational flexibility, indicating the importance of hydrophobic interactions for maintaining the conformation of such molecules.

Introduction

Lipopolysaccharide (LPS) is a characteristic component of the outer membrane of Gram-negative bacteria and forms the outermost leaflet of the lipid bilayer of the membrane.[1–5] LPS is also known as endotoxin for its toxicity and its potent immunostimulation in higher animals. LPS is a typical inducer of innate immunity and leads to the production of various mediators such as cytokines, prostaglandins, platelet activating factor, oxygen free radicals and NO. These mediators activate and modulate the immune system to protect against infection. When a large amount of LPS is released by a severe infection of Gram-negative microbes, overproduced mediators lead to endotoxin-related symptoms such as high fever, serious inflammation, hypotension and, in serious cases, lethal shock.

LPS consists of a glycolipid component termed lipid A and a polysaccharide part. It has been unequivocally proven that lipid A is the chemical entity responsible for the biological activity of LPS by our total synthesis of *Escherichia coli* lipid A (**1**) (Fig. 1).[6,7] We have also synthesized LPS from Re-mutant bacteria (Re-LPS),[8] which contains two 3-deoxy-D-manno-2-octulosonic acid (Kdo) residues linked to lipid A and various structural analogues of lipid A. Biological tests of synthetic analogues led us to conclude that hydrophobic acyl groups in lipid A play a critical role for the expression of activity.[9–13]

The tetraacyl lipid A **2**, designated as precursor Ia[14] or lipid IV_A,[15] corresponds to a lipid A component from LPS of a temperature-sensitive mutant of *Salmonella typhimurium*[16] and was identified as a key biosynthetic precursor of LPS. Interestingly, the tetraacyl biosynthetic precursor **2** shows endotoxic activity in mice but acts as a potent antagonist in suppressing the action of LPS in human systems.[9–13] By contrast, precursor-type analogue **3** with shorter acyl chains, which possesses four (*R*)-3-hydroxydecanoic acids in place of (*R*)-3-hydroxytetradecanoic acids in **2**, shows neither endotoxic nor antagonistic activities.[11] We assumed that the hydrophobic interaction between the acyl groups in lipid A should be important in maintaining its particular molecular conformation and such a conformation may be recognized by LPS binding proteins such as CD14, toll like receptor 4 (TLR4)–MD-2 complex and CD55.[1–5]

Conformations of lipid A and LPS have so far been investigated mainly using X-ray powder-diffraction and Fourier-transform and attenuated total reflectance infrared spectroscopy to estimate the approximate molecular shapes responsible for the activity.[5,17–24] Only X-ray crystallographic data of a complex of FhuA and *E. coli* K12 LPS provided a precise LPS conformation of the molecular level before the present study.[25,26] Molecular modeling studies of lipid A and LPS have also been reported.[22,23,27–32] The dihedral angles of the glycosidic bonds of some models coincide with the X-ray crystallographic data but the inclination of the lipid A backbone to acyl moieties did not.[27–29] Conformational studies of lipid A in organic solvents using NMR afforded different results from those obtained by the above X-ray analyses.[32,33]

We therefore started independent conformational analysis of lipid A by NMR in aqueous media to obtain the three-dimensional structure in relation to its biological functions. In this paper, we describe direct NMR evidence leading to the elucidation of 1) the monomolecular conformation and 2) a supramolecular assembly of biosynthetic precursor-type lipid A **2** in aqueous micelles. We also analyzed the monomolecular conformation of a biologically inactive analogue **3** in both aqueous solutions and micelles. The importance of hydrophobic interaction of acyl groups for maintaining the conformation of the molecule of lipid A is also discussed.

Results

Conformations of oligosaccharides in solution have generally been determined by NMR using information regarding the atom distances between monosaccharide residues and dihedral angles around the glycosidic bonds.[34] The former information is obtained from NOE analysis and the latter is determined from heteronuclear coupling constants, $^3J_{C,H}$, across glycosidic linkages.[35] It had been difficult to obtain $^3J_{C,H}$ values because of the low natural abundance of the ^{13}C isotope. Recent development of J-HMBC 2D experiments overcame this disadvantage.[36–38] Combinations of hetero half-filtered total correlation spectroscopy (HETLOC) and phase-sensitive HMBC have also proved to be useful in determining $^3J_{C,H}$ values.[39,40] These methods, however, failed to give a reliable result with the natural abundance of ^{13}C owing to the low solubility of the lipid A analogue **2**. Hence, we decided to synthesize two biosynthetic precursor derivatives, ^{13}C-labeled at the 1′- and 6-positions, to overcome the solubility problem. Having already completed the synthesis of 6-^{13}C-labeled **2** and its short chain analogue **3**,[41] in the present study we synthesized the 1′-^{13}C-labeled derivatives of **2** and **3**.

† Electronic supplementary information (ESI) available: other NMR data, synthetic data and rotatable 3D crystal structure diagrams of conformation **i**, conformation **ii**, conformation short, supramolecule **I** and supramolecule **II**. See http://www.rsc.org/suppdata/ob/b4/b410544c/

DOI: 10.1039/b410544c

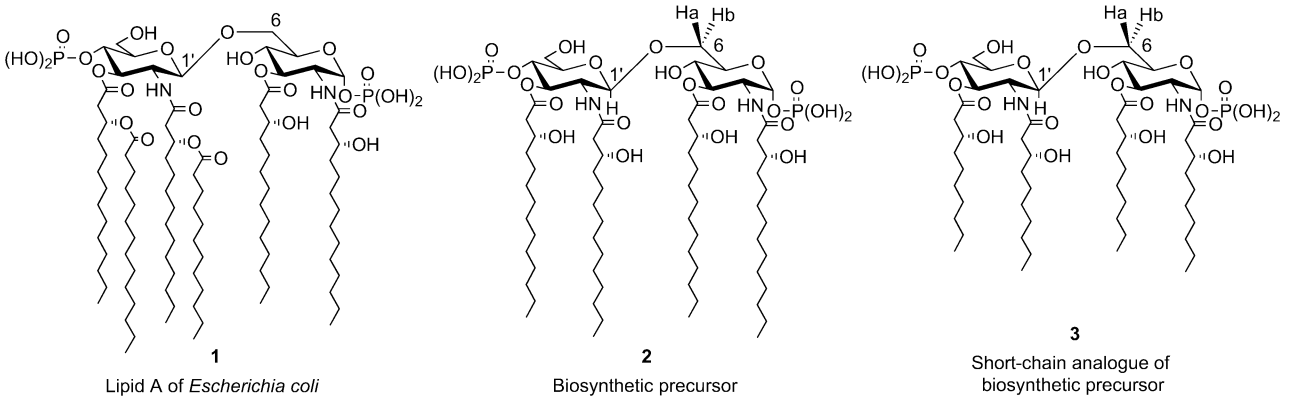

Fig. 1 The chemical structures of *Escherichia coli* lipid A, the biosynthetic precursor-type lipid A and a short chain analogue of the biosynthetic precursor.

Synthesis of ^{13}C-labeled compounds

The 1′-^{13}C-labeled derivative of **2** was *de novo* synthesized as shown in Schemes 1 and 2. The 1,6:2,3-dianhydro-(1-^{13}C) mannopyranose **4** was prepared from commercially available D-(1-^{13}C)glucose as described previously for the 6′-labeled compound.[41] The benzyl group of **4** was changed to an acetyl group. An azido group was then introduced at the 2-position and the resulting 2-azido anhydroglucose **7** was treated with phenyl trimethylsilyl sulfide and zinc iodide to give the thioglycoside **8** (α : β = 5 : 1). Removal of the acetyl groups of **8** followed by benzylidenation afforded **10**. The azido group of **10** was reduced and then a 2,2,2-trichloroethoxycarbonyl (Troc) group was introduced to the resulting 2-amino group as a stereochemical auxiliary for β-selective glycosylation to give **11**. (*R*)-3-Benzyloxytetradecanoic acid[11] **20** was introduced to the 3-position of the α-anomer of **11**, which was chromatographically isolated from the anomeric mixture. Regioselective reductive opening of the benzylidene group of **12** and subsequent cleavage of the thioglycoside gave the 1,4-dihydroxy compound **14**. We have traditionally used the trichloroacetimidate method for glycosylation with *N*-Troc glucosaminyl donors. In the present study however, we used a glycosyl phosphate as a donor[42–46] in order to reduce the number of reaction steps. In this way, compound **14** was phosphorylated using Watanabe's reagent[47] to give the bisphosphate **15**, which was to be used as the glycosyl donor (Scheme 1). The glycosylation of the acceptor **16** with **15** proceeded smoothly, using trimethylsilyltrifluoromethane

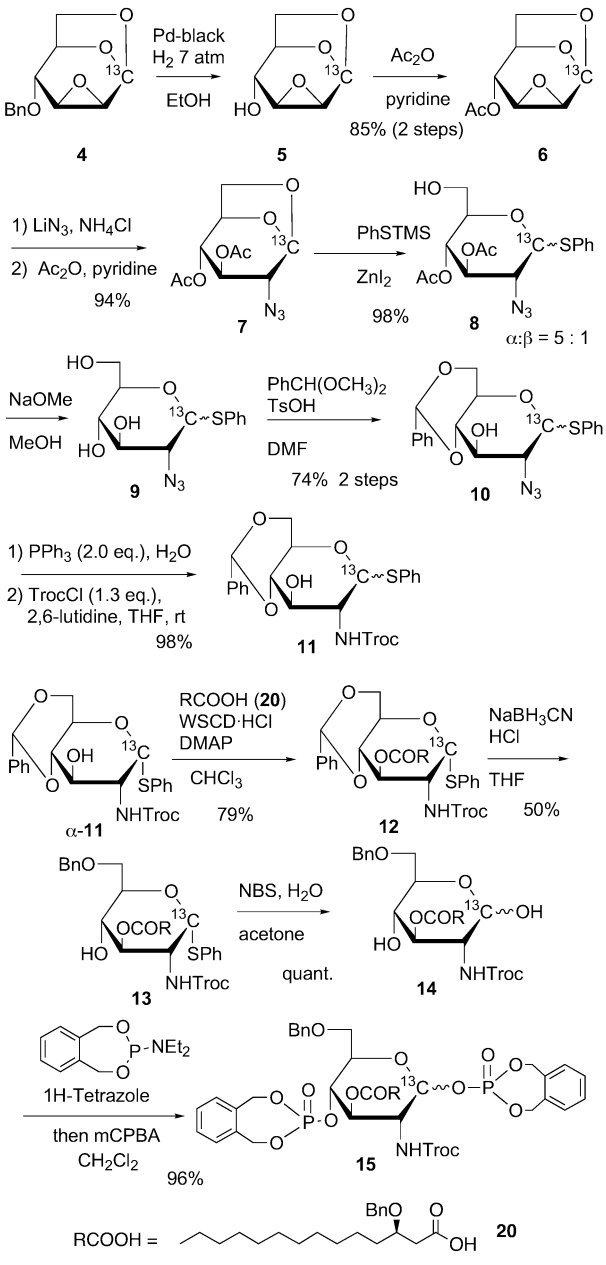

Scheme 1 Synthesis of ^{13}C-labeled glycosyl donor.

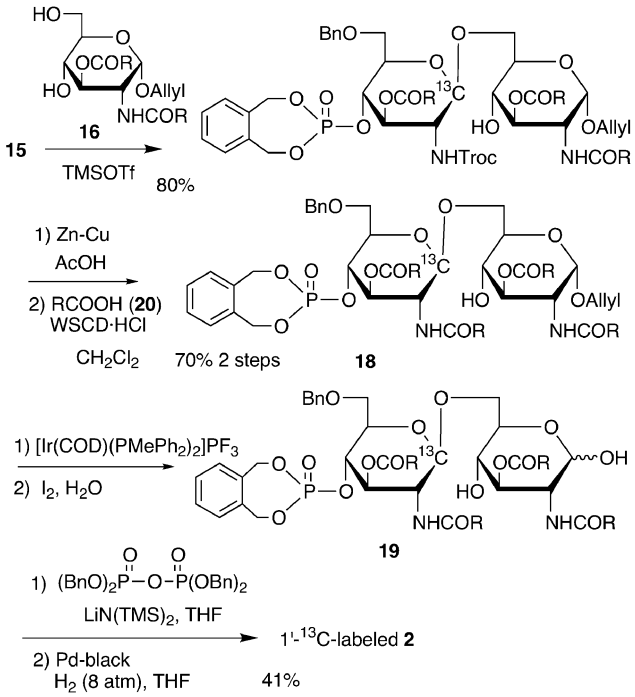

Scheme 2 Synthesis of 1′-^{13}C-labeled biosynthetic precursor.

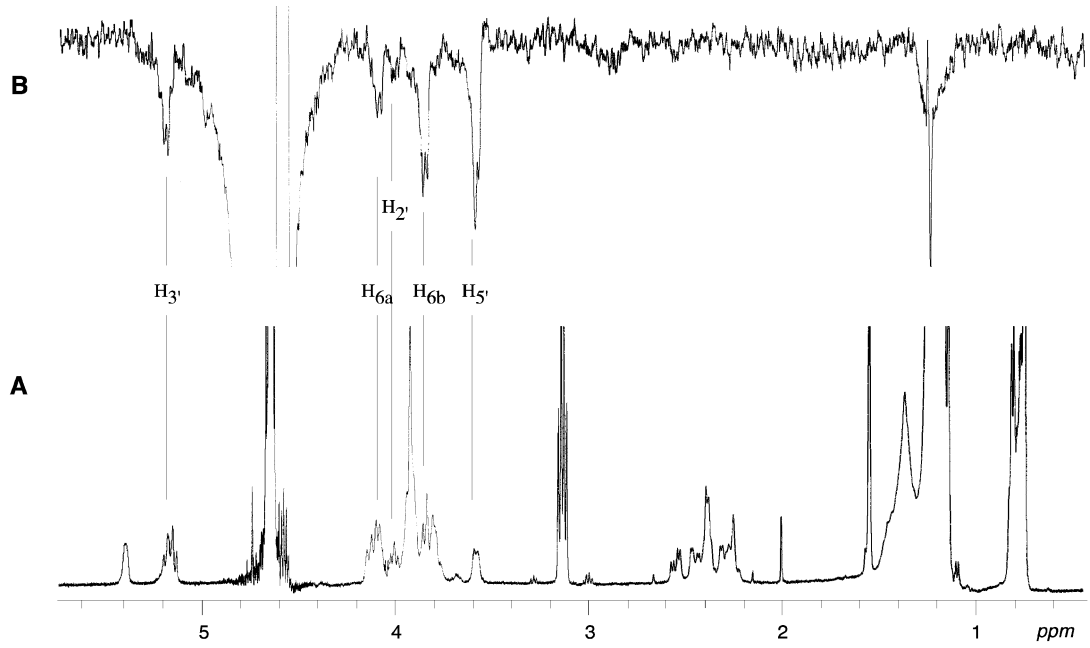

Fig. 2 One-dimensional NMR spectra of unlabeled **2**. A: ^{1}H NMR spectrum (500 MHz). B: GOESY spectrum irradiated at 4.67 ppm ($H_{1'}$) with a mixing time of 100 ms.

sulfonate (TMSOTf), to give the disaccharide **17** in a good yield. Cleavage of the *N*-Troc group was followed by *N*-acylation to give fully the acylated disaccharide **18**. The allyl group of **18** was then removed and the resulting 1-hydroxy group was phosphorylated. Final deprotection of all the benzyl-type protective groups by catalytic hydrogenation gave the desired 1′-^{13}C-labeled **2**. The 1′-^{13}C-labeled derivative of the short chain analogue **3** was synthesized in a similar manner.

Conformation of the biosynthetic precursor 2

Compound **2** gave well-resolved ^{1}H NMR spectra in DMSO-d_6[33] but broad signals in D_2O, owing to the short spin–spin relaxation time (T_2) due to self-aggregation. Addition of SDS to aqueous solutions of amphiphilic glycolipids has been shown to give sharp NMR signals of their hydrophilic parts.[48–50] Well-resolved sharp spectra were obtained of **2** in SDS-micelles (Fig. 2, A) and the following precise analysis thus became possible. Micelle conditions under a large excess of SDS employed in this work are regarded as a simulation of the amphiphilic environment on the cell surface membrane of both bacteria and host animals. Under such amphiphilic conditions, the conformation of lipid A must be regulated by the packing of acyl chains in lipid layers or micelles owing to the lipophilic aggregation.

The labeled and unlabeled **2** gave identical ^{1}H NMR spectra, except for the splitting of the proton(s) on the labeled position in the former ($^1J_{C6,H6} = 150$ and 143.5 Hz for 6-^{13}C-**2**, and $^1J_{C1',H1'} =$ 163.9 Hz for 1′-^{13}C-**2**), respectively. The concentration of SDS, at 88 mM, was far higher than its critical micelle point (8.2 mM),[51] hence the solution was considered to be under micelle conditions. Proton signals of **2** in SDS-d_{25}–D_2O were assigned by COSY and NOESY. The distinct signal of ^{13}C-labeled C_6 at δ 68.5 made it easy to assign the signals of H_4 and H_5 by the use of a ^{13}C–^{1}H HMBC spectrum. Protons at C_6 and $C_{6'}$ were assigned on the basis of Ohrui's empirical rule.[52] The clear assignment for all protons, $C_{1'}$ (δ 102.7) and C_6 (δ 68.5) of **2**, shows that there are no conformational changes in SDS-d_{25}–D_2O which are slower than the time scale of NMR. Important $^nJ_{X,H}$-coupling constants which were determined are as follows. The $^3J_{H5,H6a}$ (1.4 Hz), $^3J_{P1,H1}$ (1.0 Hz) and $^3J_{P4',H4'}$ (7.2 Hz) values were obtained from ^{1}H *J*-resolutional spectroscopy. $^3J_{C6,H1'}$ (6.6 Hz) and $^2J_{C6,H5}$ (1.7 Hz) were from the splitting of the respective signals ($H_6/H_{1'}$ and H_5/H_6), both appearing as an "exclusive COSY"-like[53] cross-peak structure in the NOESY spectra of 6-^{13}C-**2** (Fig. 3, A and Fig. 3, B). The $^3J_{C1',H6a}$ (0 Hz) and $^3J_{C1',H6b}$ (4.2 Hz) values were evaluated from the NOESY spectrum of 1′-^{13}C-**2** (Fig. 3, C) in

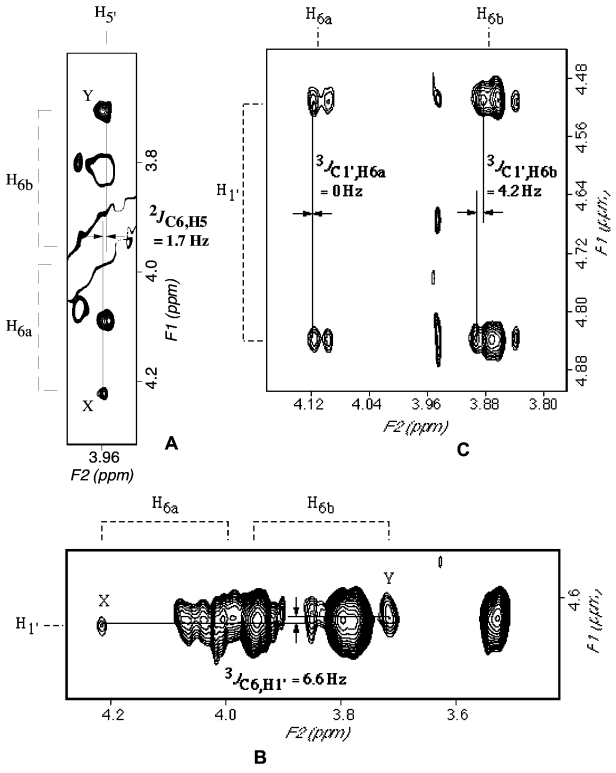

Fig. 3 NOESY (600 MHz) spectra of ^{13}C-labeled **2**. A: The correlated signals between the lower half of H_{6a}/H_5 (X) and the upper half of H_{6b}/H_5 (Y) of 6-^{13}C-**2** with a mixing time of 300 ms. Both signals are split by $^2J_{C6,H5}$ in the T_2 dimension. B: The correlated signals between the left half of $H_{6a}/H_{1'}$ (X) and the right half of $H_{6b}/H_{1'}$ (Y) of 6-^{13}C-**2** with a mixing time of 500 ms. Both signals are split by $^3J_{C6,H1'}$ in the T_1 dimension. C: The correlated signals of $H_{6a}/H_{1'}$ and $H_{6b}/H_{1'}$ of 1′-^{13}C-**2** with a mixing time of 300 ms. Both signals are split by $^3J_{C1',H6a}$ or $^3J_{C1',H6b}$ in the T_2 dimension. The slope of the linked line between the split cross peaks against the slope of diagonal peaks represents the relative sign of the coupling constants.[53]

a similar manner. These selected NMR data are summarized in Fig. 4.

Since the two glucosamine residues in **2** share normal $^4C_1$ chair conformations, as concluded from the $^3J_{H,H}$ values of the ring protons (Table 1), the rotational angles of the three bonds which determine the overall shape of the molecule, *i.e.*, C_5–C_6, C_6–O, and O–$C_{1'}$ between the two pyranosyl residues, had to be estimated.

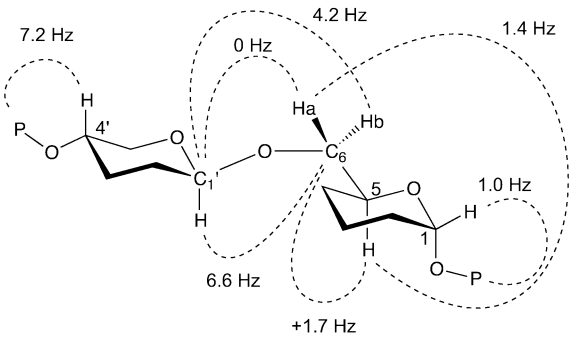

Fig. 4 Important $^nJ_{X,H}$-coupling constants of **2** for the conformational analysis. $\{\rho, \psi, \phi\} = \{-120°, -150°, -60°\}$ [ρ = (O–$C_{1'}$–O_g–C_6), ψ = ($C_{1'}$–O_g–C_6–C_5), ϕ = (O_g–C_6–C_5–O)].

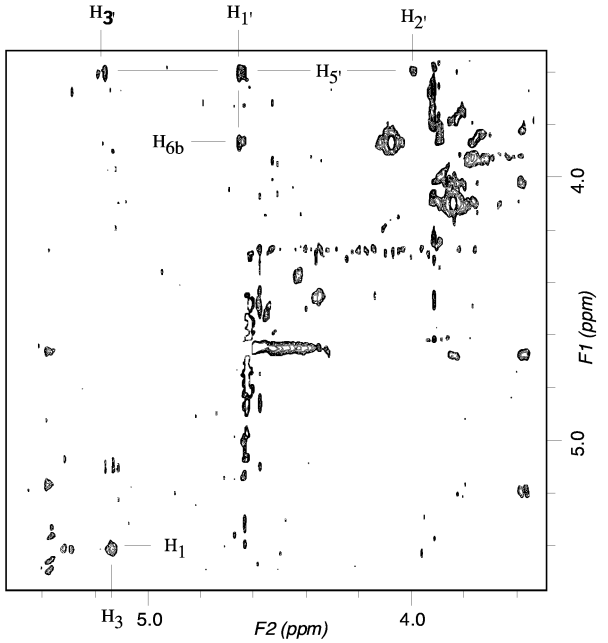

Fig. 5 T-ROESY (500 MHz) spectrum of unlabeled **2** obtained with a mixing time of 75 ms. Negative cross peaks are omitted for clarity.

The dihedral angle of the H_5–C_5–C_6–O_g bond was determined from $^2J_{C6,H5}$ and $^3J_{H5,H6a}$ values: the $^2J_{C6,H5}$ value of 1.7 Hz indicates H_5–C_5(OR)–C_6–O_gR to be in a *trans*-conformation,[54] which is also supported by the small $^3J_{H5,H6a}$ value (1.4 Hz).

The $^3J_{C6,H1'}$ value (6.6 Hz) was used for the determination of the dihedral angle of C_6–O_g–$C_{1'}$–$H_{1'}$. The large coupling constant observed shows that the conformation is either *cis* or *trans* according to the Karplus equation with Tvaroska's coefficients, $^3J_{C,H} = 5.7\cdot\cos^2\theta - 0.6\cdot\cos\theta + 0.5$, where θ is the dihedral angle of C_6–O_g–$C_{1'}$–$H_{1'}$.[55] Taking into account the observed strong NOE between H_{6b} and $H_{1'}$ (Fig. 2, B and Fig. 5), the conformation should be *cis* but never *trans*.

Rotational conformation for C_6–O_g can be drawn by two dihedral angles for H_{6a}–C_6–O_g–$C_{1'}$ and H_{6b}–C_6–O_g–$C_{1'}$, and was uniquely determined on the basis of two values, *i.e.*, 0 Hz for $^3J_{C1',H6a}$ and 4.2 Hz for $^3J_{C1',H6b}$ as follows. Since $^3J_{C,H}$ generally assumes positive values, 0 Hz for $^3J_{C1',H6a}$ should indicate the occurrence of a single conformation but not an equilibrium mixture of various conformers around the C_6–O bond. The possible dihedral angles for H_{6a}–C_6–O_g–$C_{1'}$ (±90°) and H_{6b}–C_6–O_g–$C_{1'}$ (±30° or ±140°) were calculated by putting these two $^3J_{C,H}$ values into the above Karplus equation. From the stereochemical assignment for H_{6a} (*pro-S*) and H_{6b} (*pro-R*) and the observed NOEs at $H_{6a}/H_{1'}$ and $H_{6b}/H_{1'}$, two dihedral angles for the C_6–O_g bond were concluded to be +90° and −30° for H_{6a}–C_6–O_g–$C_{1'}$ and H_{6b}–C_6–O_g–$C_{1'}$, respectively.

The orientation of the phosphates can be likewise determined by the $^3J_{P,H}$ value using the Karplus equation, $^3J_{P,H} = A\cdot\cos^2\theta - B\cdot\cos\theta$, where A (*e.g.*, 18.1) and B (*e.g.*, 4.8) are the coefficients reported in several reports[56–59] and θ is the dihedral angle of P–O–C–H. The coupling constants for $^3J_{P1,H1}$ (1.0 Hz) and $^3J_{P4',H4'}$ (7.2 Hz) show the relationships between these nuclei to be exclusively *gauche* (±60° or ±100°) and non-restricted, respectively. It should be noted here that Batley *et al.* reported the corresponding value of a deacylated LPS in D_2O to be 7.2 Hz which differs from our result.[49] This discrepancy is attributable to the different mode of aggregation and molecular

Table 1 Assignments of ^{1}H NMR (500 MHz) signals of 6-^{13}C-**2** in SDS-d_{25}–D_2O

Protons	Chemical shifts δ	Multiplicity	Coupling constants J/Hz
H1	5.41	dd	1.0, 1.0
H2	4.12	dd	9.8, 1.0
H3	5.16	dd	10.4, 9.8
H4	3.84	m	10.4[c]
H5	3.94	m	1.7, 1.4[c]
H6a(*pro-S*)[a]	4.09	ddd	150, 10.2, 1.4
H6b(*pro-R*)[a]	3.85	m	143.5, 10.2[c]
H1′	4.67	dd	11.5, 6.6
H2′	4.01	dd	11.5, 7.9
H3′	5.18	dd	9.2, 7.9
H4′	4.09	ddd	9.2, 9.2, 7.2
H5′	3.57	m	9.2[c]
H6'a(*pro-S*)[a]	3.84	m	—
H6'b(*pro-R*)[a]	3.80	m	—
acyl groups[a]			—
oxymethines (4H)	3.95, 3.94, 3.91, 3.91	m	—
methylenes (8H)	2.57, 2,47, 2.45, 2.39, 2.34, 2.31, 2.29, 2.25	m	—
other methylenes (80H)	1.50–1.14	m	—
methyl (12H)	0.86–0.75	m	—

[a] The low-field protons on C_6 and $C_{6'}$ designated 'a' were assigned to be *pro-S* according to the literature.[52] [b] Protons on the acyl groups were not completely assigned. [c] These protons have other undetermined coupling constants.

conformation (see below) owing to the different acylation patterns.

Further important conformational information was obtained from NOE data. Because there are negative correlations caused by Hartmann–Hahn effects or spin diffusions in T-ROESY spectra (Fig. 5), some positive ROESYs are not clearly observed from $H_{1'}$, such as NOEs shown in the GOESY spectrum (Fig. 2, B). Both GOESY and T-ROESY spectra were, therefore, considered complementary to the conformational analysis. From these spectra, a number of NOE signals can be seen between the protons of interglycosidic relationships, such as $H_{6a}/H_{1'}$ (medium) and $H_{6b}/H_{1'}$ (strong) as well as the normal intraglycosidic correlations of $H_{1'}/H_{3'}$ (strong), $H_{3'}/H_{5'}$ (strong) and $H_{1'}/H_{5'}$ (strong). Though the $H_{1'}$ signal (δ 4.67) is overlapped by HDO in the ^{1}H NMR spectrum, the GOESY correlations (Fig. 2, B) are apparently not those between HDO and **2** for the following reasons; 1) irradiation at HDO (δ 4.65) itself showed no GOESY signals in the region of δ 3.5–4.2; and 2) reverse irradiation at δ 3.5–4.2 gave no GOESY with HDO (δ 4.65) but with $H_{1'}$ (δ 4.67). Two interglycosidic NOEs agree with the dihedral angles around the C_6–O_g and O_g–$C_{1'}$ bonds assigned above. From these NMR data, the monomolecular conformation of **2** can be roughly drawn as illustrated in Fig. 6.

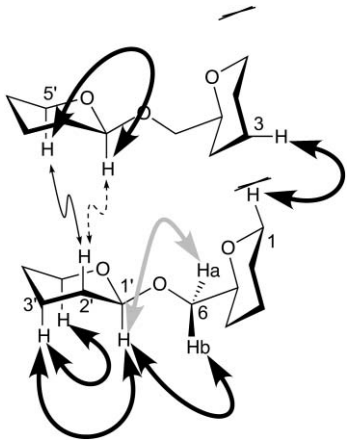

Fig. 6 Important NOE data of **2** for the conformational analysis. Bold (black), bold (gray), plain and dashed lines indicate the intensity of NOE correlations: strong, medium, weak and very weak, respectively.

Besides these intramolecular correlations used for the conformational consideration of the single molecule, the other signals observed in Fig. 2, B and Fig. 5 include the correlations of H_1/H_3 (strong), $H_{1'}/H_{2'}$ (very weak), and $H_{2'}/H_{5'}$ (weak), which cannot be explained by intramolecular interactions from the stereochemical point of view (Fig. 6). These positive cross peaks in T-ROESY can be regarded as direct NOEs[60] and are, hence, rationally assigned to be intermolecular ROESY signals. These intermolecular ROESYs provide direct evidence of the supramolecular formation of lipid A in aqueous micelles.

Based on the conformational information obtained so far from NMR, molecular modeling was studied next. The geometry of monomolecular lipid A was optimized by the molecular mechanics calculations under AMBER* force field[61] with a generalized Born/surface area (GB/SA) continuum water solvation model[62] using MacroModel version 7.0 (Schrödinger Inc.). Since NMR provided only the data for the conformation of the saccharide part, the geometry of the acyl moieties was determined as the energy minimized conformation fulfilling the structural information shown in Fig. 4 and Fig. 6. For the ester and amide groups the s-*trans* conformations were employed. The monomolecular conformation **i** [H_5–C_5–C_6–O_g (172°), H_{6a}–C_6–O_g–$C_{1'}$ (+84°) and C_6–O_g–$C_{1'}$–$H_{1'}$ (+18°)] was thus obtained as a stable conformer (Fig. 7, A) without any constraints, though **i** was not a global energy minimum. The more stable conformer of **2** [H_5–C_5–C_6–O_g (178°), H_{6a}–C_6–O_g–$C_{1'}$ (+112°) and C_6–O_g–$C_{1'}$–$H_{1'}$ (+52°)] was found by pure Low mode conformational search.

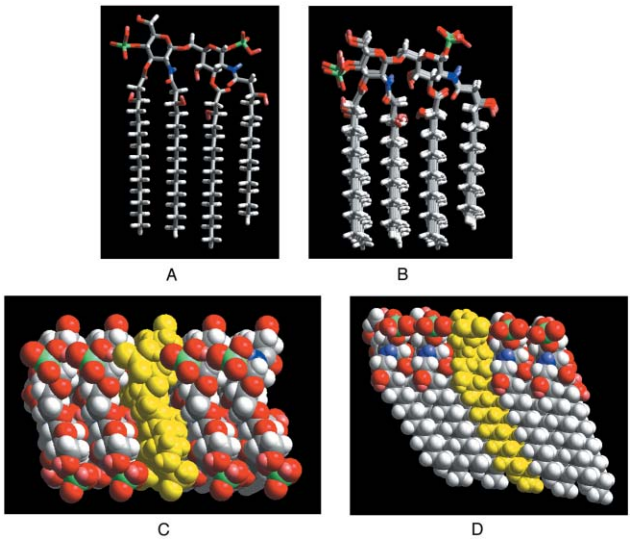

Fig. 7 Supramolecular and molecular conformation of **2** (conformer **I**). Elements are distinguished by color: carbon (white), hydrogen (white), oxygen (red), nitrogen (blue) and phosphorus (green). The CPK model is used for visualization in C and D. A: single molecular conformation **i**. B: front view of a supramolecule, consisting of 5 molecules of **2**. C: top view of the supramolecule. A central single molecule is shown in yellow. D: side view of the supramolecule.

The monomolecular conformation **i** was then used to construct supramolecular structures. Since intermolecular NOEs at H_1/H_3 and $H_{2'}/H_{5'}$ cannot occur simultaneously, the NOE data may possibly account for the fluctuation of supramolecular aggregation or the presence of two types of aggregations. In the present study, the geometry of the supramolecular assembly was optimized independently for two intermolecular relationships, assuming that one particular assembly exhibits an intermolecular NOE at H_1/H_3 (conformer **I**) and the other shows that of $H_{2'}/H_{5'}$ (conformer **II**).

A supramolecule with five lipid A molecules was chosen as a model. The geometrical restraints H_5–C_5–C_6–O_g (180°), H_{6a}–C_6–O_g–$C_{1'}$ (+90°), and C_6–O_g–$C_{1'}$–$H_{1'}$ (0°), as well as the intermolecular distance restraints, H_1/H_3 (2.5 Å) and $H_{1'}/H_{2'}$ (4.0 Å), were applied to generate supramolecular structure **I**. An additional dihedral restraint was also applied for P_1–O–C_1–H_1 to be −60°. The geometry of **I** was then minimized without any constraints under Amber* force field (Fig. 7).

The two phosphate groups occupy *gauche* and *syn* positions against the respective vicinal protons (averaged dihedral angles of P–O–C–H are −49° for P_1 and −8° for $P_{4'}$) and the averaged dihedral angles are H_5–C_5–C_6–O_g (169°), H_{6a}–C_6–O_g–$C_{1'}$ (+88°), H_{6b}–C_6–O_g–C_1 (−32°) and C_6–O_g–$C_{1'}$–$H_{1'}$ (+15°). The averaged distances of $H_{6a}/H_{1'}$ showing medium NOE, and $H_{6b}/H_{1'}$ showing strong NOE are 2.9 Å and 2.1 Å, respectively. The averaged distances of H_1/H_3, $H_{1'}/H_{2'}$ and $H_{2'}/H_5$ in the most stable supramolecule **I** were 3.0 Å, 4.0 Å and 5.8 Å, respectively.

One further supramolecular structure **II** was constructed by a similar calculation protocol using another monomolecular geometry **ii** [H_5–C_5–C_6–O_g (170°), H_{6a}–C_6–O_g–$C_{1'}$ (+90°) and C_6–O_g–$C_{1'}$–$H_{1'}$ (+17°)] (Fig. 8, A), whose conformation in acyl moieties and the information for intermolecular distances $H_{2'}/H_{5'} \cong H_{1'}/H_{2'} < H_1/H_3$ differs slightly from that of **I**. Minimization of the supramolecule generated using **i** and these intermolecular distances, afforded the disordered structure. The optimized supramolecular assembly **II** is shown in Fig. 8. The conformations of phosphate group P_1 and $P_{4'}$ were found to be a mixture of *gauche* and *syn* [P_1: two *gauche* (−34.0°) and three *syn* (+8.2°),[63] $P_{4'}$: four *gauche* (−50.0°) and one *syn* (−6.0°)]. The average dihedral angles for bonds between pyranose rings

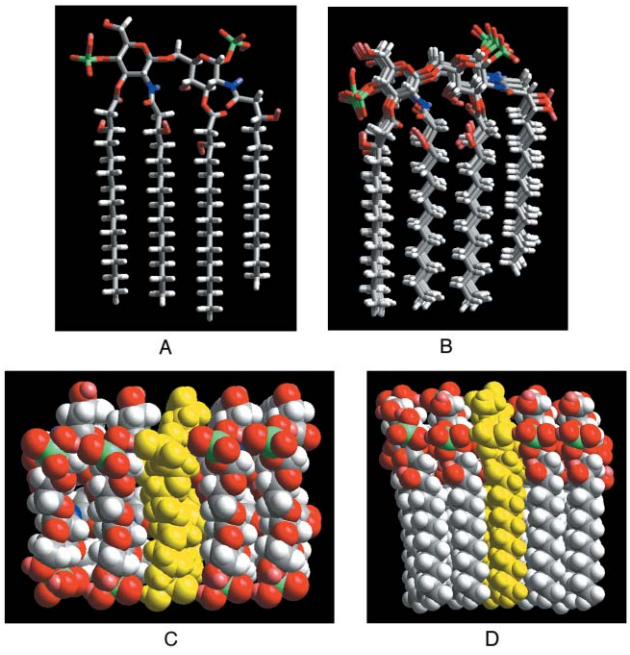

Fig. 8 Supramolecular and molecular conformation of **2** (conformer **II**). Elements are distinguished by color: carbon (white), hydrogen (white), oxygen (red), nitrogen (blue) and phosphorus (green). The CPK model is used for visualisation in C and D. A: single molecular conformation **ii**. B: front view of the supramolecule, consisting of 5 molecules of **2**. C: top view of the supramolecule. Centered molecule is shown in yellow. D: side view of the supramolecule.

are H_5–C_5–C_6–O_g (+161.4°), H_{6a}–C_6–O_g–$C_{1'}$ (+97.3°), H_{6b}–C_6–O_g–C_1 (−22.3°) and C_6–O_g–$C_{1'}$–$H_{1'}$ (+38.8°).

The average internuclear distances around the glycosidic linkage are 3.2 Å for $H_{6a}/H_{1'}$ and 2.1 Å for $H_{6b}/H_{1'}$. The averaged distances of H_1/H_3, $H_{1'}/H_{2'}$ and $H_{2'}/H_5$ in the most stable supramolecule **II** were 3.6 Å, 2.3 Å and 2.6 Å, respectively.

On the basis of two independent intermolecular NOE and other NMR data, two types of aggregation **I** and **II** were illustrated. It is likely that supramolecule **I** is the major one, as estimated from the relative intensity of the two intermolecular NOEs of H_1/H_3 and $H_{2'}/H_{5'}$, though this value cannot be directly related to the population of **I** and **II**. The supramolecular models obtained by the calculation were in good agreement with the observed data. At present no conclusion can be made as to whether supramolecular forms **I** and **II** are present close together in each single aggregate or separately from each other in different aggregates. In addition, it is not known whether **2** forms mixed aggregates with SDS or forms separate aggregates. In any case, the supramolecules shown in Fig. 7 and Fig. 8 are assumed to be present in an aqueous media in not such fragmentary forms, but as parts of higher aggregates such as micelles or liposome-like double-layered particles.

Conformation of short chain analogue of the biosynthetic precursor

The short chain analogue **3** in D_2O gave analysable ^{1}H-NMR spectra. The $^3J_{H5,H6a}$ (2.5 Hz) and $^3J_{H5,H6b}$ (3.1 Hz) values were obtained from ^{1}H *J*-resolutional spectroscopy of non-labeled **3** in D_2O. These results indicated the presence of *trans*-conformation (77% population) and two *gauche*-conformations (−60°: 13% population, 60°: 10% population) in *H5*–C_5(OR)–C_6–O_gR. The populations of conformers were determined by Ohrui's equation[52] The $^3J_{C6,H1'}$ (1.5 Hz) was obtained from the splitting of the signal ($H_6/H_{1'}$) in the NOESY spectra of 6-^{13}C-**3**. Taking into account the exoanomeric effect, the dihedral angle of C_6–O_g–$C_{1'}$–$H_{1'}$ was deduced to be +60°. The $^3J_{C1',H6b}$ value (3.1 Hz) was evaluated from the NOESY spectrum of 1′-^{13}C-**3**, whereas the $^3J_{C1',H6a}$ could not be determined because of overlapping NOE (H1′-H6a) and TOCSY signals (H1′-H4′). Strong NOE signals were observed on $H_{6a}/H_{1'}$ and $H_{6b}/H_{1'}$. The possible dihedral angles for H_{6b}–C_6–O_g–$C_{1'}$ were, therefore, −40° or −130°. The coupling constants for $^3J_{P1,H1}$ (3.2 Hz) and $^3J_{P4',H4'}$ (7.0 Hz) show the relationships between these nuclei to be exclusively *gauche* and non-restricted, respectively. In conclusion, several conformers of **3** exist in D_2O and the molecule freely rotates at least around the C_5–C_6 bond.

The coupling constants in SDS-d_{25}–D_2O were different from those in D_2O. Important $^nJ_{X,H}$-coupling constants of **3** in SDS-d_{25}–D_2O are as follows: $^3J_{H5,H6a}$ (0 Hz), $^3J_{H5,H6b}$ (5.9 Hz), $^3J_{C6,H1'}$ (2.9 Hz), $^3J_{C1',H6a}$ (0.7 Hz), $^3J_{C1',H6b}$ (1.8 Hz), $^3J_{P1,H1}$ (2.0 Hz) and $^3J_{P4',H4'}$ (7.1 Hz). A number of intramolecular NOE signals including $H_{6a}/H_{1'}$ (medium) and $H_{6b}/H_{1'}$ (strong) were observed. From these values and NOE data, the conformation of **3** in SDS-d_{25}–D_2O was deduced to be C_6–O_g–$C_{1'}$–$H_{1'}$: +45°, H_{6a}–C_6–O_g–$C_{1'}$: +100°, H_{6b}–C_6–O_g–$C_{1'}$: −25°, H_5–C_5(OR)–C_6–*OgR*: *trans* (53% population) and *gauche* (−60 °: 47% population). Molecular mechanics calculation of monomolecular **3** afforded the stable conformer [C_6–O_g–$C_{1'}$–$H_{1'}$ (+54 °), H_{6a}–C_6–O_g–$C_{1'}$ (+104 °), H_5–C_5–C_6–O_g (179 °)] without any constraints (Fig. 9). The calculated conformer is hence identical with the observed major one.

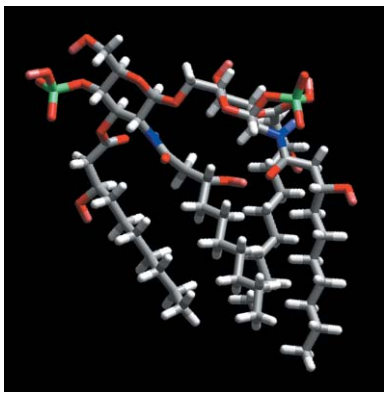

Fig. 9 Stable conformer of the short-chain analogue **3**.

Contrary to the observation for **2**, compound **3** does not form a supramolecular assembly in SDS-micelles, as judged from the fact that no intermolecular NOE signals were observed.

Discussions

The present study provides the first NMR evidence of lipid A conformation in aqueous media. The biosynthetic precursor lipid A **2** forms two types of supramolecular assembly, which may be in a kind of dynamic equilibrium. It should be noted here that the observed monomolecular conformation of **2**, especially the geometry around the glycosidic bond C_6–O_g–$C_{1'}$–$H_{1'}$, is not energetically the most favored as indicated by the molecular mechanistic calculation of the single molecule. A set of the torsion angles of **2** derived from the observed conformation in the SDS-micelles was $\{\rho, \psi, \phi\} = \{-120°, -150°, -60°\}$ [ρ = (O–$C_{1'}$–O_g–C_6), ψ = ($C_{1'}$–O_g–C_6–C_5), ϕ = (O_g–C_6–C_5–O)]. The observed dihedral angle C_6–O_g–$C_{1'}$–$H_{1'}$ (*ca.* 0°) (ρ = −120°) was significantly low in view of the exoanomeric effect, which favors the dihedral angle of the glycosidic bond to be *ca.* 40–60° (C_6–O_g–$C_{1'}$–$H_{1'}$). A set of dihedral angles of the most stable conformer of monomeric **2** calculated here was $\{\rho, \psi, \phi\} = \{-67°, -128°, -63°\}$. The distortion at C_6–O_g–$C_{1'}$–$H_{1'}$ in the micelle should be compensated by the formation of a supramolecular structure; the distorted monomolecular conformation may become a favorable one by making the intermolecular hydrophobic interaction largest. The alignment of both phosphate moieties of the assembling molecules is another characteristic of this arrangement (Fig. 7C and Fig. 8C),

which may have a further function to stabilize the supramolecule, particularly in the presence of multivalent cations.

Before the present study, only X-ray crystallographic data of the complex of FhuA and *E. coli* K12 LPS provided the empirical information of lipid A conformation.[25,26] The dihedral angles around the glycosidic bonds in the lipid A part were $\{\rho, \psi, \phi\} = \{-75°, -150°, -108°\}$. Energy minimization of the hexaacylated lipid A part derived from the reported X-ray data under Amber* force field led to similar torsion angles, except ϕ $\{\rho, \psi, \phi\} = \{-72°, -132°, -77°\}$. This result suggests that the complex formation of *E. coli* K12 LPS with FhuA probably distorted the ϕ angle in its lipid A part. The conformation around the glycosidic bonds of the biosynthetic precursor **2** in aqueous SDS-micelles obtained as above is essentially the same as that of the lipid A part in K12 LPS observed in X-ray analysis, since the differences of all dihedral angles between the two works are less than 60°.

Seydel, Brandenburg and coworkers have studied the supramolecular structures and intrinsic conformations of lipid A derivatives in relation to their biological activities.[5,17–21,24] The present supramolecular models of **2** are in good accordance with their observations, as follow. They reported an aggregated lamellar structure of the biosynthetic precursor lipid A **2** in water, indicating the cross-sectional areas of hydrophilic and hydrophobic parts are almost the same. The small tilt angle (*ca.* 10°) of the backbone with respect to the direction of acyl chains was observed in the same aggregates of **2**.[21] They also reported a highly hydrated 1-phosphate and a weakly hydrated 4′-phosphate in lipid A and LPS.[18] These lead to a molecular shape in which 1-phosphate is more accessible to the aqueous phase than the 4′-phosphate.

Several molecular mechanics and molecular dynamics studies have also been reported for conformational study of lipid A and LPS.[22,23,27–31] As for the torsion angles of the glycosidic bonds, the models of both Labischinski *et al.* and Obst and coworkers are consistent with the X-ray crystallographic data of the FhuA-*E. coli* K12 LPS complex.[23,27–29] Those models, however, have a reverse inclination (the 1-phosphate being close to the bilayer and the 4′-phosphate being directed to the aqueous phase), which is inconsistent with the X-ray crystallographic data and the observations of Seydel *et al*.

The importance of hydrophobic interactions in the formation of lipid A conformation was also proven by our NMR study of the short-chain analogue **3**. The short-chain analogue **3** takes several conformations in water and SDS-d_{25}–D_2O, as indicated by NMR. The hydrophobic interaction between the acyl groups of **3** may not be strong enough to maintain any particular conformation, though the major conformation in the SDS-micelles [$\{\rho, \psi, \phi\} = \{-75°, -150°, -60°\}$] is similar to the stable conformations of **2** and *E. coli* lipid A **1**, as described above.

The lack of both endotoxic and antagonistic activities in **3** can be explained by its low tendency to bind to LPS receptors owing to its conformational flexibility, where a large entropic loss would arise for the binding of **3** to the LPS receptors. This explanation is also supported by a TLC blotting assay using a lipid A monoclonal antibody (mAb A6), which has been proven to recognise the hydrophilic part of lipid A.[64] The antibody recognises the *E. coli* lipid A **1** and the biosynthetic precursor **2** but does not bind to **3**.[65] The importance of hydrophobic interaction in maintaining the conformation of lipid A is also well understood, by comparing the present result with our previous NMR study of **2** in DMSO.[33] In this solvent, where no hydrophobic affinity operates, two flexible conformers of **2** were detected, both of which were similar to two conformers of **3** in SDS-micelle, respectively.

As described, the conformations of tetraacyl lipid A **2** and its regular supramolecular assembly in SDS were determined by NMR analysis. NMR spectra of hexaacyl *E. coli* lipid A (**1**) in aqueous media remained broad even after the addition of SDS, indicating its lower fluidity compared to that of **2**. A similar arrangement was observed for Re-LPS, which is composed of a hexaacyl lipid A and two additional sugar units, by using X-ray diffraction and atomic force microscopic studies.[66] These results suggest that LPS in the bacterial outer membrane forms a similar assembly, which may be further stabilized by the multivalent cations such as Ca^{2+} and Mg^{2+}. The strong tendency of lipid A molecules to form such a supramolecular structure is expected to be the origin of the mechanical stability of the bacterial outer membrane.

Recently, Seydel *et al.* revealed that monomeric lipid A and LPS prepared by a dialysis procedure showed no activity, whereas aggregates at the same concentrations were biologically active.[67] These results suggest that monomeric lipid A and LPS might be conformationally flexible due to the lack of intermolecular hydrophobic interactions and hence is not recognised by the LPS receptor system. The particular conformation of lipid A in the supramolecular assembly should be recognized by the LPS receptor system.

Triantafilou reported that LPS triggers the recruitment of receptors in the LPS receptor system, *e.g.*, TLR4-MD2, CD14, CD55, CD11b/CD18, CD81 and CXCR4, within membrane microdomains on the cell membrane.[68] The driving force for the cluster formation is not yet known. Seydel *et al.* reported lipopolysaccharide-binding protein-mediated intercalation of lipid A to phospholipid membranes.[19] The present study suggests that lipid A incorporated in the membrane still forms a supramolecular assembly, which may accumulate in membrane microdomains such as lipid rafts, since lipid A has many saturated fatty acids. Lipid A binding proteins, therefore, may gather on membrane microdomains and trigger LPS signaling.

Experimental

Materials

The 6-^{13}C- labeled **2** and **3** were previously synthesized starting from commercially available D-(6-^{13}C)-glucose.[41] The 1′-^{13}C-labeled derivatives of **2** and **3** were newly synthesized. The details of the synthesis are described in the Electronic Supplementary Information†. Deuterated sodium dodecyl sulfate (SDS-d_{25}) was purchased from Aldrich.

NMR spectroscopy

The sample solution of **2** was prepared by addition of 8.27 mg (0.026 mmol) of SDS-d_{25} to 0.33 μmol of **2** in 0.30 mL of D_2O (99.96% D). The solution of **3** was prepared by a similar method with or without SDS-d_{25}. All NMR spectra were measured at 303 K with JEOL JNM-Lambda 500 or Varian Unity-plus 600 spectrometers and analyzed using the Felix® program (version 97.0, Molecular Simulations). Proton chemical shifts were referenced to the proton of HDO (4.65 ppm). COSY and heteronuclear multiple-bond correlation (HMBC) spectra were obtained by standard measurement procedures. NOESY spectra were collected with a mixing time ranging from 300–1500 ms, while transverse rotating-frame Overhauser effect spectroscopy (T-ROESY)[60] and gradient enhanced nuclear Overhauser effect spectroscopy (GOESY)[69] were performed with 50–175 ms and 100–300 ms mixing time, respectively. The water signal was suppressed by the DANTE (delays alternating with nutation for tailored excitation) pulse.[70] Each spectrum size was 1024–4096 complex points in the T_2 dimension and 256–512 complex points in T_1. Two-fold zero-filling was carried out in both dimensions, and the data were processed using exponential or shifted sine-bell window functions before transformation.

Calculations

The molecular mechanics calculations were carried out under the all-atom AMBER* force field[61] with generalized

Born/surface area (GB/SA) continuum water solvation model[62] using MacroModel version 7.0 (Schrödinger Inc.). The energy minimization was performed by truncated Newton conjugate gradient minimization (the convergence threshold was 0.05 kJ^{-1} Å mol^{-1}).

Acknowledgements

The authors thank Mr S. Adachi and Dr K. Li of the NMR laboratory of the department for their skillful measurements and Dr E. Fukushi of the GC-MS & NMR laboratory, Hokkaido University, for helpful discussions. S. K. is grateful to Prof. R. R. Schmidt at Universität Konstanz, Germany, for his valuable suggestions about the use of SDS-micelles in the NMR study of lipid A. This work was partly supported by a Grant-in-Aid for Scientific Research on Priority Areas No. 09273102 from the Ministry of Education, Science, Sports and Culture, Japan. We also appreciate the financial support of "Research for the Future" Program No. 97L00502 from the Japan Society for the Promotion of Science.

References

1 A. J. Ulmer, E. Th. Rietschel, U. Zähringer and H. Heine, *Trends Glycosci. Glycotechnol.*, 2002, **14**, 53–68.
2 C. Alexander and U. Zähringer, *Trends Glycosci. Glycotechnol.*, 2002, **14**, 69–86.
3 C. Alexander and E. Th. Rietschel, *J. Endotoxin Res.*, 2001, **7**, 167–202.
4 *Endotoxin in Health and Disease*, eds. H. Brade, S. M. Opal, S. N. Vogel and D. C. Morrison, Marcel Dekker, New York, Basel, 1999.
5 U. Seydel and K. Brandenburg, in *Bacterial Endotoxic Lipopolysaccharides*, eds. D. C. Morrison and J. L. Ryan, CRC Press, Florida, 1992, vol 1, p. 225.
6 M. Imoto, H. Yoshimura, T. Shimamoto, N. Sakaguchi, S. Kusumoto and T. Shiba, *Bull. Chem. Soc. Jpn.*, 1987, **60**, 2205–2214.
7 M. Imoto, H. Yoshimura, M. Yamamoto, T. Shimamoto, S. Kusumoto and T. Shiba, *Bull. Chem. Soc. Jpn.*, 1987, **60**, 2197–2204.
8 H. Yoshizaki, N. Fukuda, K. Sato, M. Oikawa, K. Fukase, Y. Suda and S. Kusumoto, *Angew. Chem., Int. Ed.*, 2001, **40**, 1475–1480.
9 M. Oikawa, A. Wada, H. Yoshizaki, K. Fukase and S. Kusumoto, *Bull. Chem. Soc. Jpn.*, 1997, **70**, 1435–1440.
10 W.-C. Liu, M. Oikawa, K. Fukase, Y. Suda, H. Winarno, S. Mori, M. Hashimoto and S. Kusumoto, *Bull. Chem. Soc. Jpn.*, 1997, **70**, 1441–1450.
11 K. Fukase, Y. Fukase, M. Oikawa, W.-C. Liu, Y. Suda and S. Kusumoto, *Tetrahedron*, 1998, **54**, 4033–4050.
12 W.-C. Liu, M. Oikawa, K. Fukase, Y. Suda and S. Kusumoto, *Bull. Chem. Soc. Jpn.*, 1999, **72**, 1377–1385.
13 H. Loppnow, H. Brade, I. Durrbaum, C. A. Dinarello, S. Kusumoto, E. Th. Rietschel and H. D. Flad, *J. Immunol.*, 1989, **142**, 3229–3238.
14 T. Hansen-Hagge, V. Lehmann and O. Luderitz, *Eur. J. Biochem.*, 1985, **148**, 21–27.
15 M. S. Strain, I. M. Armitage, L. Anderson, K. Takayama, N. Qureshi and C. R. H. Raetz, *J. Biol. Chem.*, 1985, **260**, 16089–16098.
16 V. Lehmann, *Eur. J. Biochem.*, 1977, **75**, 257–266.
17 K. Brandenburg, H. Mayer, M. H. J. Koch, J. Weckesser, E. Th. Rietschel and U. Seydel, *Eur. J. Biochem.*, 1993, **218**, 555–563.
18 K. Brandenburg, S. Kusumoto and U. Seydel, *Biochem. Biophys. Acta*, 1997, **1329**, 183–201.
19 T. Gustmann, A. B. Schromm, M. H. J. Koch, S. Kusumoto, K. Fukase, M. Oikawa, U. Seydel and K. Brandenburg, *Phys. Chem. Chem. Phys.*, 2000, **2**, 4521–4528.
20 A. B. Schromm, K. Brandenburg, H. Loppnow, A. P. Moran, M. H. Koch, E. Th. Rietschel and U. Seydel, *Eur. J. Biochem.*, **267**, 2008–2013.
21 U. Seydel, M. Oikawa, K. Fukase, S. Kusumoto and K. Brandenburg, *Eur. J. Biochem.*, 2000, **267**, 3032–3039.
22 H. Labischinski, E. Vorgel, W. Uebach, R. P. May and H. Bradaczek, *Eur. J. Biochem.*, 1990, **190**, 359–363.
23 M. Kastowsky, T. Gutberlet and H. Bradaczek, *Eur. J. Biochem.*, 1993, **217**, 771–779.
24 U. Seydel, H. Labischinski, M. Kastowsky and K. Brandenburg, *Immunobiology*, 1993, **187**, 191–211.
25 A. D. Ferguson, E. Hofmann, J. W. Coulton, K. Diederichs and W. Welte, *Science*, 1998, **282**, 2215–2220.
26 A. D. Ferguson, W. Welte, E. Hofmann, B. Lindner, O. Holst, J. W. Coulton and K. Diederichs, *Structure Fold. Des.*, 2000, **8**, 585–592: we found that the stereochemistry of the 3′-*o*-acyloxyacyl group of K12 LPS in the X-ray crystallographic analysis was incorrect. The X-ray data showed the 3′-*o*-acyloxyacyl group has an *S*-configuration, whereas other acyloxyacyl and hydroxyacyl groups have an *R*-configuration. We hence checked the chirality of 3-hydroxytetradecanoic acid obtained from K12 LPS and did not detect the *S*-isomer at all (O. Holst, K. Fukase, unpublished results). The *S*-configuration of the 3′-*o*-acyloxyacyl group in the X-ray analysis should be corrected as *R*-configuration.
27 H. Labischinski, G. Barnickel, H. Bradaczek, D. Naumann, E. T. Rietschel and P. Giesbrecht, *J. Bacteriol.*, 1985, **162**, 9–20.
28 M. Kastowsky, A. Sabisch, T. Gutberlet and H. Bradaczek, *Eur. J. Biochem.*, 1991, **197**, 707–716.
29 S. Obst, M. Kastowsky and H. Bradaczek, *Biophys. J.*, 1997, **72**, 1031–1046.
30 P. Pristovsek and J. Kidric, *J. Med. Chem.*, 1999, **42**, 4604–4613.
31 V. Frecer, B. Ho and J. L. Ding, *Eur. J. Biochem.*, 2000, **267**, 837–852.
32 Y. Wang and R. I. Hollingsworth, *Biochemistry*, 1996, **35**, 5647–5654.
33 M. Oikawa, T. Shintaku, H. Yoshizaki, K. Fukase, S. Adachi, K. Lee and S. Kusumoto, *Bull. Chem. Soc. Jpn.*, 2001, **74**, 1455–1461.
34 T. B. Grindley, in *Glycoscience*, eds. B. Fraser-Reid, K. Tatsuta and J. Thiem, Springer, Berlin, 2001, vol 1, p. 3 and references cited therein..
35 I. Tvaroska and F. R. Taravel, *Adv. Carbohydr. Chem. Biochem.*, 1995, **51**, 15–61.
36 W. Willker and D. Leobfritz, *Magn. Reson. Chem.*, 1995, **33**, 827–830.
37 T. Tokunaga, H. Seki, H. Utsumi, N. Nakakoshi and K. Yamaguchi, *Anal. Sci.*, 1999, **15**, 1157–1158.
38 N. Iida-Tanaka, K. Fukase, H. Utsumi and I. Ishizuka, *Eur. J. Biochem.*, 2000, **267**, 6790–6797.
39 N. Matsumori, M. Murata and K. Tachibana, *Tetrahedron*, 1995, **51**, 12229–12238.
40 N. Matsumori, D. Kaneko, M. Murata, H. Nakamura and K. Tachibana, *J. Org. Chem.*, 1999, **64**, 866–876.
41 M. Oikawa, T. Shintaku, H. Sekljic, K. Fukase and S. Kusumoto, *Bull. Chem. Soc. Jpn.*, 1999, **72**, 1857–1867.
42 S. Hashimoto, T. Honda and S. Ikegami, *J. Chem. Soc., Chem. Commun.*, 1989, 685–687 .
43 G.-J. Boons, A. Burton and P. Wyatt, *Synlett*, 1996, 310–312.
44 S. Hashimoto, H. Sakamoto, T. Honda and S. Ikegami, *Tetrahedron Lett.*, 1997, **38**, 5181–5184.
45 V. Hariprasad, G. Singh and I. Tranoy, *Chem. Commun.*, 1998, 2129–2130.
46 O. J. Plante, R. B. Andrade and P. H. Seeberger, *Org. Lett.*, 1999, **1**, 211–214.
47 Y. Watanabe, Y. Komoda, K. Ebisuya and S. Ozaki, *Tetrahedron Lett.*, 1990, **31**, 255–256.
48 E. F. Hounsell, *Prog. Nucl. Magn. Reson. Spectrosc.*, 1995, **27**, 445–474.
49 M. Batley, N. H. Packer and J. W. Redmond, *Biochemistry*, 1982, **21**, 6580–6586.
50 S. M. Strain, S. W. Fesik and I. M. Armitage, *J. Biol. Chem.*, 1983, **258**, 2906–2910.
51 P. Mukerjee and K. J. Mysels, in *Critical Micelle Concentrations in Aqueous Surfactant Systems*, National Bureau of Standards, Washington, 1971.
52 H. Ohrui, Y. Nishida, M. Watanabe, H. Hori and H. Meguro, *Tetrahedron Lett.*, 1985, **26**, 3251–3254.
53 C. Griesinger, O. W. Sorensen and R. R. Ernst, *J. Am. Chem. Soc.*, 1985, **107**, 6394–6396.
54 C. A. Podlasek, J. Wu, W. A. Stripe, P. B. Bondo and A. S. Serianni, *J. Am. Chem. Soc.*, 1995, **117**, 8635–8644.
55 I. Tvaroska, M. Hricovini and E. Petrakova, *Carbohydrate Res.*, 1989, **189**, 359–362.
56 A. A. Bothner-By and W.-P. Trautwein, *J. Am. Chem. Soc.*, 1971, **93**, 2189–2192.
57 B. Donaldson and L. D. Hall, *Can. J. Chem.*, 1972, **50**, 2111–2118.
58 B. J. Blackburn, R. D. Lapper and I. C. P. Smith, *J. Am. Chem. Soc.*, 1973, **95**, 2873–2878.
59 R. H. Contreras and J. E. Peralta, *Prog. Nucl. Magn. Reson. Spectrosc.*, 2000, **37**, 321–425.
60 T.-L. Hwang and A. J. Shaka, *J. Am. Chem. Soc.*, 1992, **114**, 3157–3159.
61 H. Senderowitz, C. Parish and W. C. Still, *J. Am. Chem. Soc.*, 1996, **118**, 2078–2086.
62 W. C. Still, A. Tempczyk, R. C. Hawley and T. Hendrickson, *J. Am. Chem. Soc.*, 1990, **112**, 6127–6129.

63 From the observed $^{3}J_{P,H}$, all P–O–C_1–H_1 should take a *gauche* conformation. By applying the appropriate boundary condition for P–O–C_1–H_1 (restraint at P–O–C_1–H_1 of the right terminal lipid A molecule in Fig. 9, D was −40°), all P–O–C_1–H_1 took a *gauche* conformation in molecular modeling of **II** (averaged dihedral angle was −38°).
64 L. Brade, O. Holst and H. Brade, *Infect. Immun.*, 1993, **61**, 4514–4517.
65 K. Fukase, M. Oikawa, Y. Suda, W.-C. Liu, Y. Fukase, T. Shintaku, H. Sekljic, H. Yoshizaki and S. Kusumoto, *J. Endotoxin Res.*, 1999, **5**, 46–51.
66 N. Kato, T. Sugiyama, S. Naito, Y. Arakawa, H. Ito, N. Kido, M. Ohta and K. Sasaki, *Mol. Microbiol.*, 2000, **36**, 796–805.
67 M. Mueller, B. Lindner, S. Kusumoto, K. Fukase, A. B. Schromm and U. Seydel, *J. Biol. Chem.*, 2004, **279**, 26307–26313.
68 M. Triantafilou, K. Brandenburg, S. Kusumoto, K. Fukase, A. Mackie, U. Seydel and K. Triantafilou, *Biochem. J.*, 2004, **381**, 527–536.
69 J. Stonehouse, P. Adell, J. Keeler and A. J. Shaka, *J. Am. Chem. Soc.*, 1994, **116**, 6037–6038.
70 E. R. P. Zuiderweg, K. Hallenga and E. T. Olejniczak, *J. Magn. Reson.*, 1986, **70**, 336–343.